Biointerface Research in Applied Chemistry
Open-Access Journal (ISSN: 2069-5837)

Article
Volume 13, Issue 4, 2023, 364
https://doi.org/10.33263/BRIAC134.364

Impact of Zinc Substitution on AC Conductivity Behaviors of Hexagonal Ba-Ni Ferrite Nanoparticle

A. H. AL-Hammadi [1], Sadiq. H. Khoreem [1,2*]

[1] Physics Department, Faculty of Science, Sana'a University, Sana'a, Yemen
[2] Department of Optometry and Vision Science, Faculty of Medical Sciences, Al-Razi University, Sana'a, Yemen
* Correspondence: khoreems@yahoo.com, sadiqkhoreem@alraziuni.edu.ye;

Scopus Author ID 57571836200
Received: 29.06.2022; Accepted: 18.07.2022; Published: 7.10.2022

Abstract: The influence of composition on electrical conductivity (σac) as a function of temperature and frequency is investigated for BaNi2-xZnxFe16O27 nanoparticle ferrite with the variation of zinc concentration (x = 0, 0.4, 0.8, 1.2, 1.6 and 2) synthesized by the conventional ceramic process. With an increase in zinc content from 0.0 to 2 at the selected frequency, AC conductivity (σac) decreases. AC conductivity results specify the hopping conduction mechanisms in the studied temperature range. The electrical conductivity (σac) properties as a function of frequency (100 KHz to 1KHz) within the temperature range (293–486 K) have been investigated. The ac conductivity shows both temperature and frequency dependence, with a relatively stronger dependence in the lower and higher frequency ranges, respectively. Also, the results of ac conductivity show a dispersion with frequency. The dispersion decreases as the temperature increases. The universal power law is observed in this dispersion. The dispersion of ac conductivity was explained based on Koop's model. Also, it is found that σac(ω) obeys Jonscher's universal power law, σac(ω) = Aωs with s < 1. The results have been analyzed with reference to various theoretical models. The correlated barrier hopping model (CBH) process is found to be the dominant conduction mechanism for charge carrier transport within the investigated temperature range. The experimental result demonstrates that AC conductivity бac) also increases with increasing frequency.

Keywords: AC conductivity; Zinc substitution; Ba-Ni hexa-ferrites; nanoparticle.

1. Introduction

Barium ferrites became the most important technological applications due to their high frequency. The ferrite's properties strongly depend on the microstructure and composition of these ferrites. Also, the synthesis method is important in obtaining good-quality ferrites [1]. Qian Liu *et al*. [2] prepared the Ba $La_xNi_2Fe_{16-x}O_{27}$ ferrites by the ceramic method. Their structural and magnetic characteristics were discussed in relation to the variation of La rare earth in Barium nickel ferrites. They have found that the X-ray diffraction patterns confirmed Pure BaW phase formation for all samples. There is more correlation between these compositions' ac conductivity and the dielectric constant. In those systems of hexagonal, the ac conductivity and the constant dielectric increase with increasing temperature. D. El Kony *et al.* [3] investigated the effect of Mg-doping on the dielectric behavior of $BaZn_{2-x}MgxFe_{16}O_{27}$ W-type hexagonal ferrites as frequency functions, temperature, and composition, prepared by the ceramic method. They discovered that the dielectric constant frequency dependence displayed two distinct behavior patterns: normal dispersion at low temperatures and aberrant

behavior at very high temperatures. This abnormal behavior may be explained based on Rezlescu and Rezlescu's assumption, which ascribes this abnormal behavior to a collective contribution of two types of charge carriers to polarization. The dielectric characteristics and initial magnetic permeability of $BaCo_{2-x}Ni_xFe_{16}O_{27}$ ferrites made using the ceramic technique were reported by A.M. Abo El Ata et al. [4].

They have found that Ni substitution resulted in dielectric constant and dielectric loss tangent increase with increasing nickel ions substitution. The current study explores similar issues in pristine composition $BaNi_2Fe_{16}O_{27}$ and effects of non-magnetic Zn^{2+} ion-substituted on the electrical conductivity of ($BaNi_{2-x}Zn_xFe_{16}O_{27}$; x = 0.0,0.4, 0.8, 1.2, 1.6, and 2.0).

2. Materials and Methods

The ceramic method synthesized the samples of BaNi2–xZnxFe16O27 ferrites. The composition samples have been prepared by mixing $BaCO_3$, NiO, ZnO, and Fe_2O_3 according to their respective stoichiometric ratios. Further details, as mentioned earlier [5,6] and shown in figure.1, the sample powder was pressed under a pressure of 3toon/cm^2 at room temperature to form a disc for measuring the AC properties. After that, these discs were sintered at 1250 K for 6 hours and slowly cold to room temperature by turning the furnace off. Finally, the discs were polished to obtain smooth, uniform parallel plate surfaces, and a thin layer of silver coated the surface as a good contacting material for electrical conductivity measurement.

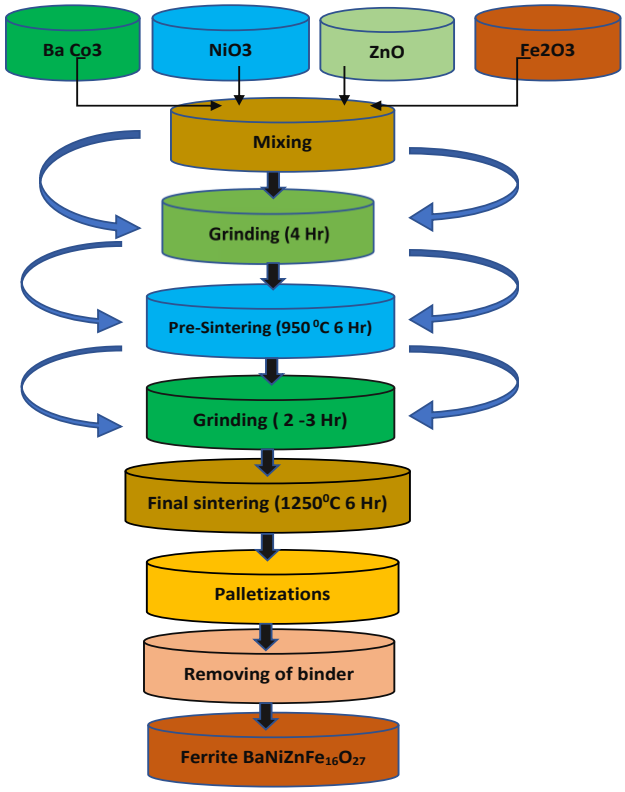

Figure 1. Schematic diagram for synthesis of Ba $Ni_{2-x}Zn_xFe_{16}O_{27}$ (x= 0.0, 0.4, 0.8, 1.2, 1.6 and 2.0) ferrites.

3. Results and Discussion

Using the relationship between the values of the dielectric constant and the dielectric loss factor, the AC conductivity of these samples was computed [1].

$$\sigma_{ac} = \omega \varepsilon_\circ \varepsilon' \tan\sigma \qquad (1)$$

where σ_{ac}, is the AC conductivity, ω is the angular frequency, ε_o represents the free-space permittivity, έ represents the dielectric constant, and tanδ represents the dielectric loss factor of the samples.

3.1. Frequency dependence of a.c. conductivity.

The variation of electrical conductivity (σac) of the $BaNi_{2-x}Zn_xFe_{16}O_{27}$ (x= 0.0, 0.4, 0.8, 1.2, 1.6, and 2.0) was performed at different temperatures with frequency was displayed in Figure 2 (a,b,c,d,e,f) shows the variation of frequency-dependent AC conductivity of ferrites at different temperatures. The AC conductivity of all the samples is found to increase with rising frequency and temperature, as has been observed. The hopping of charge carriers also rises with increasing frequency of the applied field, which raises conductivity.

According to Koop's phenomenological theory [7], which assumes that ferrite samples act as a multilayer capacitor, the increased AC conductivity with frequency and temperature is caused by the interfacial polarization. According to this hypothesis, the conductivity is caused by grain boundaries at low frequencies, but the dispersion is caused by the conducting grains at higher frequencies. Further, the Maxwell-Wagner two layers model is elaborated above phenomenological theory [8,9]. The dispersion has been observed in ac conductivity with temperature, demonstrating that conduction is a thermally induced process. At lower frequencies, the grain boundaries are more active; hence the hopping frequency of electrons between Fe^{3+} and Fe^{2+} ions is less. At high frequencies, ac conductivity curves are approaching each other, indicating the existence of various relaxation and thermally induced processes in the sample; therefore, the conductive grains become more active by promoting the hopping of electrons between Fe^{3+} and Fe^{2+} ions, increasing the hopping frequency. So, we observe the increase in conductivity with the increase in frequency. The figure shows an increase linearly with frequency and increases with temperature; additionally, the frequency dispersion of σ_{ac} in most cases has been observed. The results agree well with the theoretical relation between σ and ω; $\sigma_{ac} = A(T)\omega^{s(T)}$, Jonscher's universal power law, which is reported for a wide variety of materials, amorphous semiconductors, and glasses [10,11], where *A* and *s* are parameters dependent on temperature, ω is the angular frequency and s is the frequency exponent.

The value and behavior of the exponent *s* versus temperature tell and determine the prevailing type of conduction mechanism dominant in the material. The value of the parameter (*s*) was calculated from the slope as of lnσ versus lnω for all samples and plotted with temperature in Figure 3 (a,b,c,d,e,f). The figures show that (*s*) decreases with increasing temperature for all samples. This means that the hopping of electrons mechanism is predominant for the rest of the investigated samples to describe the ac electrical conduction for samples in this temperature range. In this model, the value of s is predicted to decrease with increasing temperature. A decrease in the power parameter with increasing temperature indicates that correlated barrier hopping (CBH) is the driving force behind charge transport. This model suggests charge transfer occurs due to thermal activation over the barrier between neighboring potential wells [12].

Conductivity is decreased, as shown in Figure 4 (e,f).

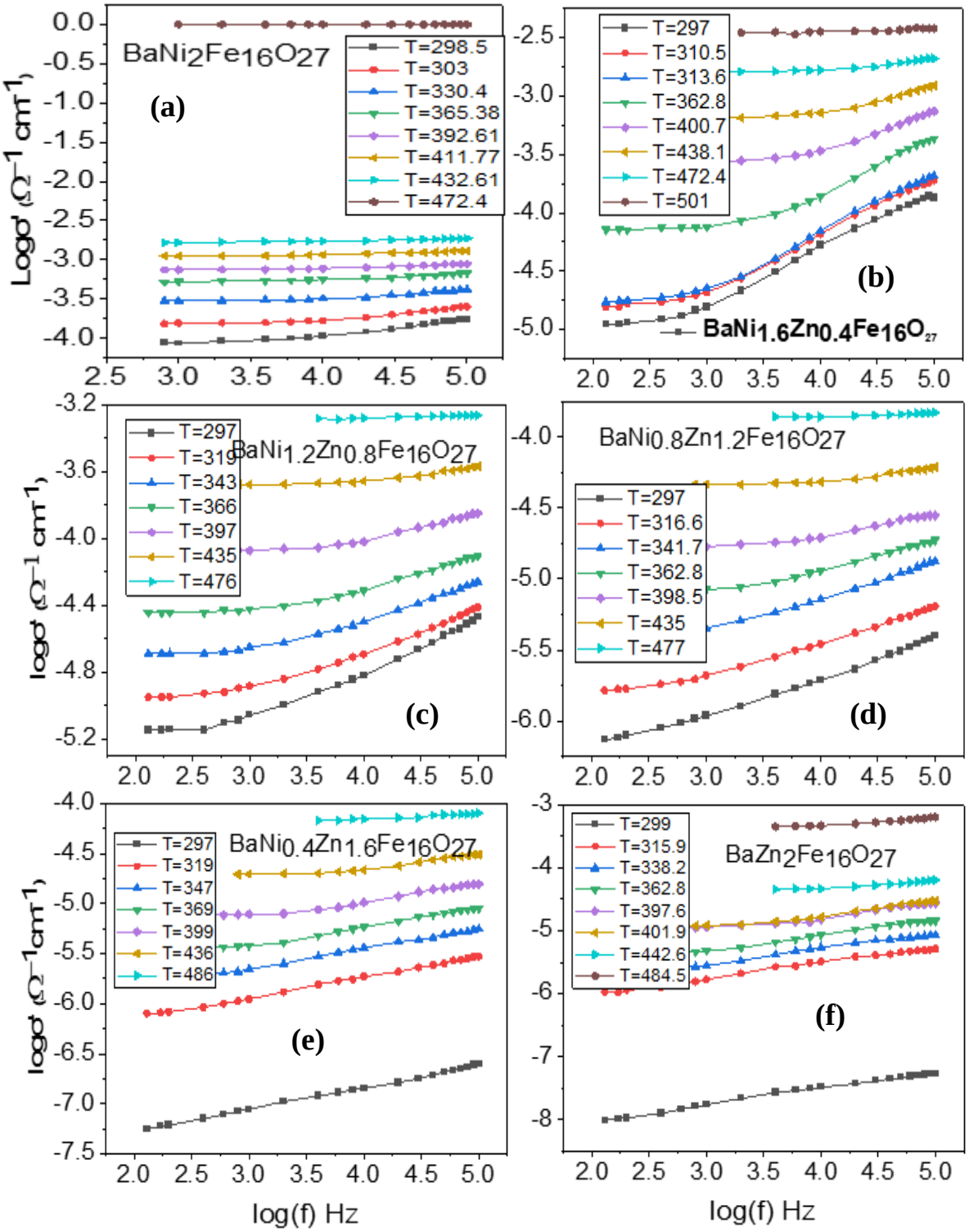

Figure 2. Frequency dependence of electrical conductivity for $BaNi_{2-x}Zn_xFe_{16}O_{27}$(x=0, 0.4, 0.8, 1.2, 1.6 and 2) (**a**); $BaNi_2Fe_{16}O_{27}$, (**b**):$BaNi_{1.6}Zn_{0.4}Fe_{16}O_{27}$, (**c**): $BaNi_{1.2}Zn_{0.8}Fe_{16}O_{27}$, (**d**): $BaNi_{0.8}Zn_{1.2}Fe_{16}O_{27}$, (**e**): $BaNi_{0.4}Zn_{1.6}Fe_{16}O_{27}$, (**f**): $BaZn_2Fe_{16}O_{27}$. at different temperatures.

In this model, the exponent n decreases as the temperature increases. Generally, a linear improvement in AC conductivity with the applied field appeared in the present synthesis samples. It deduced that in hexagonal ferrites, The frequency-induced electron hopping between Fe^{2+} and Fe^{3+} ions is responsible for the steady improvement in AC conductivity and causes the grain borders to exhibit an activist effect at low frequency, was found to have the most impact. The movement of the charge carriers was sufficient, and the grains were more active at higher frequencies [13].

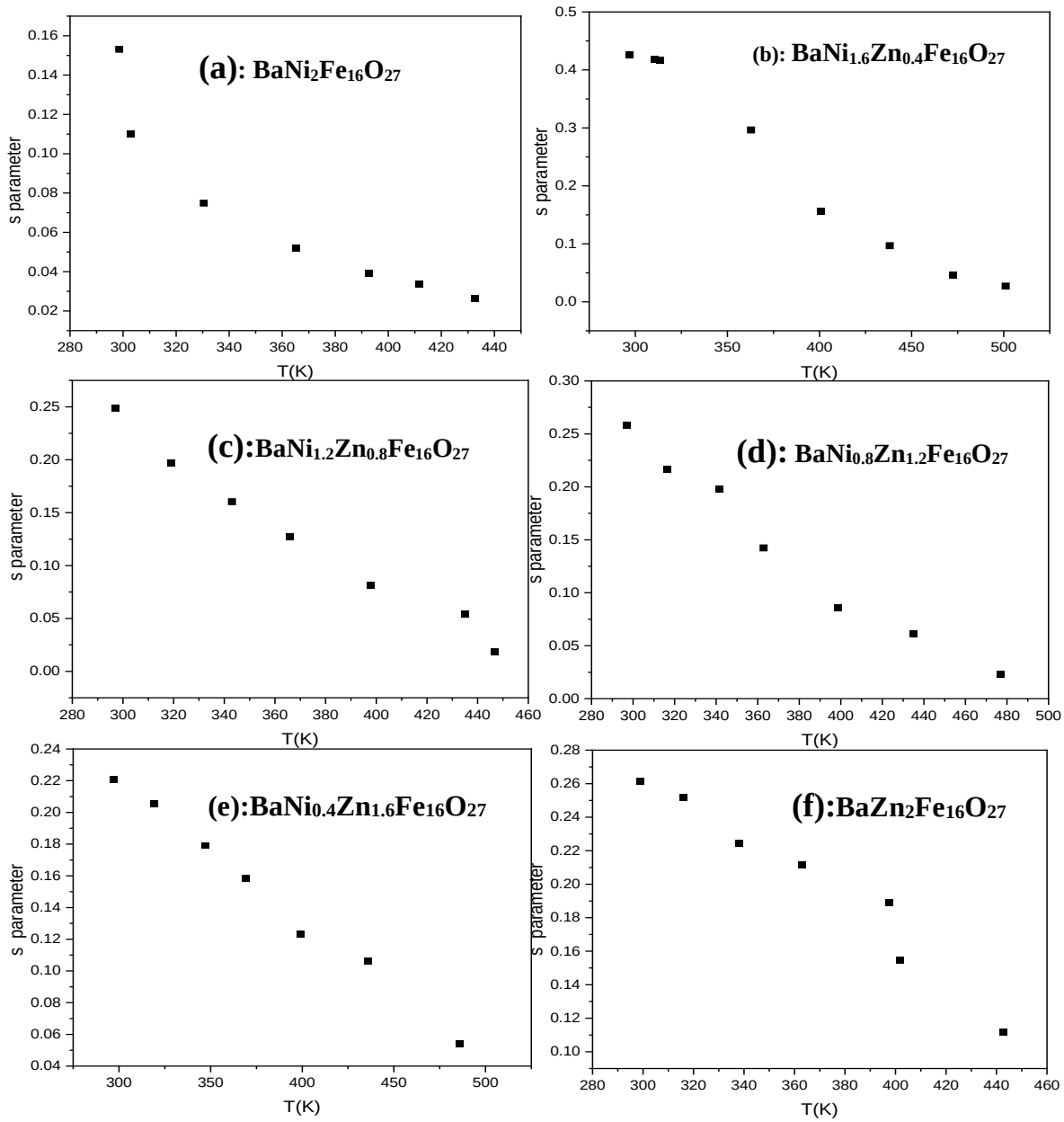

Figure 3. The variation of the parameter "s for $BaNi_{2-x}Zn_xFe_{16}O_{27}$(x=0, 0.4, 0.8, 1.2, 1.6 and 2) "(**a**); $BaNi_2Fe_{16}O_{27}$, (**b**):$BaNi_{1.6}Zn_{0.4}Fe_{16}O_{27}$, (**c**): $BaNi_{1.2}Zn_{0.8}Fe_{16}O_{27}$, (**d**): $BaNi_{0.8}Zn_{1.2}Fe_{16}O_{27}$, (**e**): $BaNi_{0.4}Zn_{1.6}Fe_{16}O_{27}$, (**f**): $BaZn_2Fe_{16}O_{27}$.with the absolute temperature T (K).

3.2. Temperature dependence of a.c. conductivity.

Figure 4 (a,b,c,d,e,f) shows the variation of the ac electrical conductivity (log σac) with the reciprocal of absolute temperature (1000/T) at different Zn content (x) and different frequencies. The data show that the ac conductivity exhibits a semiconducting behavior, where it increases with increasing temperature. It was observed that the conductivity is high at high temperatures and is frequency independent, while as the temperature decreases, the conductivity decreases and becomes frequency dependent, whereas, with increasing frequency, its values increase. The increase in the σ_{ac} conductivity with increasing temperature means that the trapped charges are liberated, which increases the exchange of electrons between Fe^{2+} and Fe^{3+} ions. Also, this increase in σ_{ac} with increasing temperature can be explained based on Koop's theory and Maxwell Wagner's model. These models inform that in the ferrite's materials, the conducting grains are separated by the thin layering of grain boundaries [14,15],

accordingly at low frequencies, the AC conductivity σ′ behavior characterizes the grain boundary, while at high frequencies, the dispersion may be attributed to the conductivity of the grains.

In the sample x=1.6 and 2, the transition temperature (Tσ where a break in logσ vs. 1000/T is obtained), both the field and applied frequency aligned the charge carriers in the same direction of the field, so the conductivity, in this case, increases with temperature. While by increasing temperature above Tσ the disturbance of the charge carriers in the different directions), the conductivity is decreased, as shown in Figure 4 (e,f).

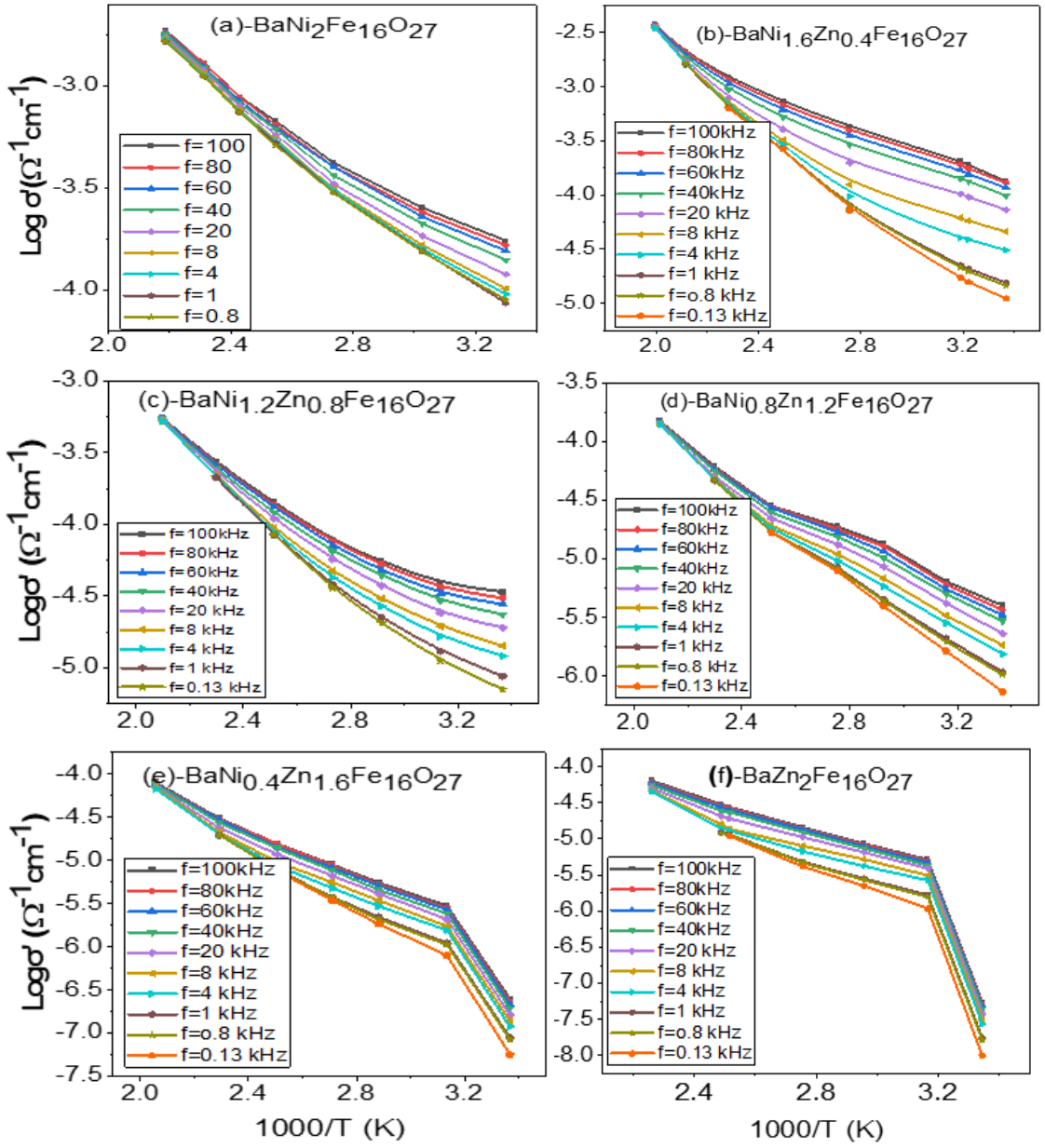

Figure 4 Temperature dependence of electrical conductivity for $BaNiFe_{16}O_{27}$ (x=0, 0.4, 0.8, 1.2, 1.6 and 2) (**a**); $BaNi_2Fe_{16}O_{27}$, (**b**):$BaNi_{1.6}Zn_{0.4}Fe_{16}O_{27}$, (**c**): $BaNi_{1.2}Zn_{0.8}Fe_{16}O_{27}$, (**d**): $BaNi_{0.8}Zn_{1.2}Fe_{16}O_{27}$, (**e**): $BaNi_{0.4}Zn_{1.6}Fe_{16}O_{27}$, (**f**): $BaZn_2Fe_{16}O_{27}$. at a different frequency.

3.3. Composition dependence of a.c. conductivity.

The relation between electrical conductivity and composition is shown in Figure 5. It is seen that the conductivity slightly increases as the zinc ions concentration increase up to

x=0.4, after that decrease. This behavior is similar to dielectric constant behaviors, as the dielectric constant is directly proportional to the square root of conductivity [16]. The compositional dependence of the electrical conductivity σ_{ac}, is shown in Figure 5 . the electrical conductivity $\sigma_{ac,}$ increase with the increase in x (zinc concentration) up to reach a maximum value at Zn =0.4; after that, a sharp decrease is noticed with further increase in zinc substitution. It was stated that the electric conduction in the studied samples is related mainly to the presence of impurities and the hopping of charge carriers [17]. Since the number of the impurity atoms is very limited, the hopping conduction mechanism plays a major role in the electric conduction and dielectric polarization process in these ferrites by electron hopping between Fe^{2+} and Fe^{3+} and hole transfer between Ni^{2+} and Ni^{3+}. It is well known that Zn^{2+} ions occupy the tetrahedral (A-sites) [18,19], Ni^{2+} ions prefer to occupy the octahedral (B-sites), while the iron ions are distributed between both A and B sites [18,20]. Therefore, the behavior of σ_{ac}, with composition in Figure 5, can be explained as follows:

The replacement of Ni^{2+} ions by Zn^{2+} ions will force some of the iron ions to migrate from A-sites to B-sites to substitute for the decrease in B-sites population [21,22]; therefore, according to the reaction $Ni^{2+}+Fe^{3+}\leftrightarrow Ni^{3+}+Fe^{2+}$, which is prevalent in ferrites containing Ni^{2+} ions, the Ni^{3+} and Fe^{2+} ions will increase. So, the hopping conduction by the electron transfer between Fe^{2+}, Fe^{3+}, and hole transfer between Ni^{3+} and Ni^{2+} will increase. Consequently, the electrical conductivity σ_{ac} increases. The above assumption is valid up to Zn=0.4. After that, the reduction of Ni content in the B-site will reduce the probability of reaction (2) and, therefore σ_{ac} decreases beyond Zn=0.4. However, the decrease noticed for the sample from x=0.8 is due to the reduction of Ni ions in the octahedral sites, which will reduce the probability of reactions $Ni^{2+}+Fe^{3+}\leftrightarrow Ni^{3+}+Fe^{2+}$ which the Ni^{3+} ions and Fe^{2+} ions will decrease so that the hopping rate will decrease, consequently the electrical conductivity decrease.

The above assumption is valid up to Zn=0.4; after that, the reduction of Ni content in the B-site will reduce the probability of reaction (2) and, therefore, σ_{ac} decreases beyond Zn=0.4. However, the decrease noticed for the sample from x=0.8 is due to the reduction of Ni ions in the octahedral sites, which will reduce the probability of reactions $Ni^{2+}+Fe^{3+}\leftrightarrow Ni^{3+}+Fe^{2+}$ which the Ni^{3+} ions and Fe^{2+} ions will decrease so that the hopping rate will decrease, consequently the electrical conductivity decrease.

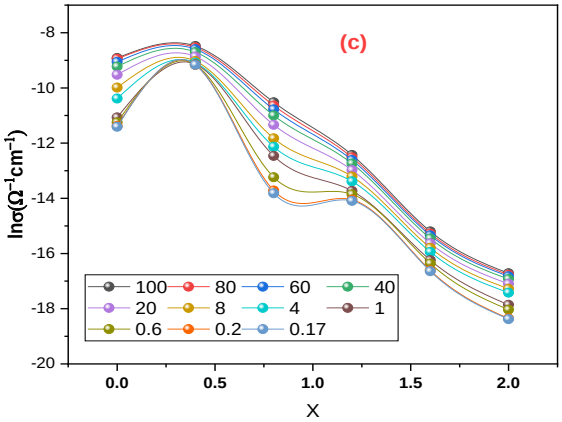

Figure 5. Relation between the conductivity, and the zinc concentration as a function of frequency for the samples $BaNi_{x-2}Zn_xFe_{16}O_{27}$; (x = 0, 0.4, 0.8, 1.2, 1.6, and 2).

The behavior of ε', σ_{ac} and $\tan\sigma$ with the composition can be explained based on the presumption [23,24] that the mechanism of the dielectric polarization is identical to that of the

electrical conduction; hence it is expected that the behavior of ε′ ,ε′′and tanσ is similar to that of σ_{ac}.

4. Conclusions

On the basis of observations and experiments, it is concluded that the substitution of Zn in the $BaNi_{2-x}Zn_xFe_{16}O_{27}$(x=0.0, 0.4, 0.8, 1.2, 1.6, and 2) nanoferrites produces appreciable changes in electrical properties. It has been discovered that temperature and frequency both improve AC conductivity. Additionally, it is discovered that $\sigma_{ac}(\omega)$ obeys the universal power law of Jonscher,$\sigma_{ac}(\omega) = A\omega^s$ with s < 1. And it is revealed that the correlated barrier hopping model (CBH) is the predominant conduction mechanism for charge carrier movement in sample material within the examined temperature range. The correlated barrier hopping (CBH) conduction mechanism successfully explained the behavior of the temperature conductivity mechanism.

Funding

This research received no external funding.

Acknowledgments

The authors would like to thank Dr. A.M. Abo El Ata and the Physics Department, Faculty of Science, Tanta University, Tanta, Egypt, for his help during the experimental measurements for the present work.

Conflicts of Interest

The authors declare no conflict of interest.

References

1. Dogra, P.; Ranote, S.; Kumar, K.; Chauhan, S.; Chauhan, G.S. New Nicotinic Acid-Based Hydrogel: Swelling and Insulin Uptake Studies. *Biointerface Res Appl Chem* **2022**, *13*, 102, https://doi.org/10.33263/BRIAC132.102.
2. Liu, Q.; Wu, C.; Wang, Y.; Liu, Y.; Zhang, H. Corrigendum: Microstructure and Magnetic Properties of Textured Barium W-Type Hexaferrite with Rare-Earth La3+ Substitution. *IOP Conf. Ser.: Mater. Sci. Eng.* **2020,** *782*, 022118, https://doi.org/10.1088/1757-899X/782/2/022118.
3. Kony, D. Dielectric Behaviour of MgZn W-Type Hexaferrite. *Egyptian Journal of Solids* **2000**, *23*, 137–146, https://doi.org/10.21608/ejs.2000.151483.
4. Kaur, M.; Kim, T.; Kim, W.S. New Frontiers in 3D Structural Sensing Robots. *Adv. Mater.* **2021**, *33*, 2002534, https://doi.org/10.1002/adma.202002534.
5. AL-Hammadi , A.H.; Khoreem , Sadiq H. Investigations on Optical and Electrical Conductivity of Ba/Ni/Zn/Fe16O27 Ferrite Nanoparticles. *Biointerface Res Appl Chem* **2022**, *13*, 168, https://doi.org/10.33263/BRIAC132.168.
6. AL-Hammadi , A.H.; Khoreem , Sadiq H. Influence of Zn+2 Doping on Dielectric Properties of BaBased Nanoferrites. *Biointerface Res Appl Chem* **2022,** 13, 256, https://doi.org/10.33263/BRIAC133.256.
7. Raddaoui, Z.; El Kossi, S.; Brahem, R.; Bajahzar, A.; Valentinovich Trukhanov, A.; Leonidovich Kozlovskiy, A.; Vladimirovich Zdorovets, M.; Dhahri, J.; Belmabrouk, H. Hopping Conduction Mechanism and Impedance Spectroscopy Analyses of $La_{0.70}Sr_{0.25}Na_{0.05}Mn_{0.70}Ti_{0.30}O_3$ Ceramic. *J Mater Sci: Mater Electron* **2021**, *32*, 16113–16125, https://doi.org/10.1007/s10854-021-06160-6.
8. Koops, C.G. On the Dispersion of Resistivity and Dielectric Constant of Some Semiconductors at Audiofrequencies. *Phys. Rev.* **1951**, *83*, 121–124, https://doi.org/10.1103/PhysRev.83.121.

9. Kurien, S.; Mathew, J.; Sebastian, S.; Potty, S.N.; George, K.C. Dielectric Behavior and Ac Electrical Conductivity of Nanocrystalline Nickel Aluminate. *Materials Chemistry and Physics* **2006**, *98*, 470–476, https://doi.org/10.1016/j.matchemphys.2005.08.080.
10. Byfield, B.N.; Hollinger, D. Andrew and the Alchemist; Doubleday: Garden City, N.Y., **1977**.
11. Assim, E.M.; El-Metwally, E.G. A Study on Electrical (Dc/Ac) Conductivity and Dielectric Characteristics of Quaternary $Ge_{50}In_4Ga_{13}Se_{33}$ Chalcogenide Thin Films. *Journal of Non-Crystalline Solids* **2021**, *566*, 120892, https://doi.org/10.1016/j.jnoncrysol.2021.120892.
12. Farid, H.M.T.; Ahmad, I.; Ali, I.; Ramay, S.M.; Mahmood, A.; Murtaza, G. Dielectric and Impedance Study of Praseodymium Substituted Mg-Based Spinel Ferrites. *Journal of Magnetism and Magnetic Materials* **2017**, *434*, 143–150, https://doi.org/10.1016/j.jmmm.2017.03.039.
13. Li, Z.; Senanayak, S.P.; Dai, L.; Kusch, G.; Shivanna, R.; Zhang, Y.; Pradhan, D.; Ye, J.; Huang, Y.; Sirringhaus, H.; *et al*. Understanding the Role of Grain Boundaries on Charge-Carrier and Ion Transport in $Cs_2AgBiBr_6$ Thin Films. *Adv. Funct. Mater*. **2021**, *31*, 2104981, https://doi.org/10.1002/adfm.202104981.
14. Mazen, S.A.; Abdel-Daiem, A.M. IR Spectra and Dielectric Properties of Cu–Ge Ferrite. *Materials Chemistry and Physics* **2011**, *130*, 847–852, https://doi.org/10.1016/j.matchemphys.2011.09.017.
15. Ahmad, I.; Shah, S.M.; Zafar, M.N.; Ashiq, M.N.; Tang, W.; Jabeen, U. Synthesis, Characterization and Charge Transport Properties of Pr–Ni Co-Doped $SrFe_2O_4$ Spinel for High Frequency Devices Applications. *Ceramics International* **2021**, *47*, 3760–3771, https://doi.org/10.1016/j.ceramint.2020.09.233.
16. El Hiti, M.A.; Abo El Ata, A.M. Semiconductivity in $Ba_2Ni_{2-x}Zn_xFe_{12}O_{22}$ Y-Type Hexaferrites. *Journal of Magnetism and Magnetic Materials* **1999**, *195*, 667–678, https://doi.org/10.1016/S0304-8853(99)00120-1.
17. Chen, X.; Li, C.; Xu, Y.; Dolocan, A.; Seward, G.; Van Roekeghem, A.; Tian, F.; Xing, J.; Guo, S.; Ni, N.; *et al*. Effects of Impurities on the Thermal and Electrical Transport Properties of Cubic Boron Arsenide. *Chem. Mater.* **2021**, *33*, 6974–6982, https://doi.org/10.1021/acs.chemmater.1c02006.
18. Bhunia, A.K.; Pradhan, S.S.; Bhunia, K.; Pradhan, A.K.; Saha, S. Study of the Optical Properties and Frequency-Dependent Electrical Modulus Spectrum to the Analysis of Electric Relaxation and Conductivity Effect in Zinc Oxide Nanoparticles. *J Mater Sci: Mater Electron* **2021**, *32*, 22561–22578, https://doi.org/10.1007/s10854-021-06742-4.
19. Sagayaraj, R.; Aravazhi, S.; Chandrasekaran, G. Review on Structural and Magnetic Properties of (Co–Zn) Ferrite Nanoparticles. *Int Nano Lett* **2021**, *11*, 307–319, https://doi.org/10.1007/s40089-021-00343-z.
20. Tatarchuk, T.; Shyichuk, A.; Sojka, Z.; Gryboś, J.; Naushad, Mu.; Kotsyubynsky, V.; Kowalska, M.; Kwiatkowska-Marks, S.; Danyliuk, N. Green Synthesis, Structure, Cations Distribution and Bonding Characteristics of Superparamagnetic Cobalt-Zinc Ferrites Nanoparticles for Pb(II) Adsorption and Magnetic Hyperthermia Applications. *Journal of Molecular Liquids* **2021**, *328*, 115375, https://doi.org/10.1016/j.molliq.2021.115375.
21. Jahan, N.; Khandaker, J.I.; Liba, S.I.; Hoque, S.M.; Khan, M.N.I. Structural Analysis through Cations Distributions of Diamagnetic Al^{3+} Ions Substituted Ni-Zn-Co Ferrites. *Journal of Alloys and Compounds* **2021**, *869*, 159226, https://doi.org/10.1016/j.jallcom.2021.159226.
22. Verma, R.; Kane, S.N.; Tiwari, P.; Modak, S.S.; Tatarchuk, T.; Mazaleyrat, F. Ni Addition Induced Modification of Structural, Magnetic Properties and Antistructural Modeling of $Zn_{1-X}Ni_xFe_2O_4$ (x = 0.0 - 1.0) Nanoferrites. *Molecular Crystals and Liquid Crystals* **2018**, *674*, 130–141, https://doi.org/10.1080/15421406.2019.1578519.
23. Saafan, S.A.; El-Nimr, M.K.; Hussein, M.M.; K.Omar, M. FTIR, DC, and AC Electrical Measurements of Mg Zn Nano-Ferrites and Their Composites with Polybenzoxazine. *Appl. Phys. A* **2021**, *127*, 800, https://doi.org/10.1007/s00339-021-04947-2.
24. Haq, A.; Anis-ur-Rehman, M. Structural, Morphological and Electrical Analysis of Dual Doped Sr-Hexaferrite Nanoparticles. *Physica B: Condensed Matter* **2021**, *601*, 412445, https://doi.org/10.1016/j.physb.2020.412445.